Theor Chem Acc (2006) 115: 136–144
DOI 10.1007/s00214-005-0048-2

REGULAR ARTICLE

James R. Rustad · William H. Casey

A molecular dynamics investigation of the titration of a trivalent aqueous ion

Received: 5 May 2005 / Accepted: 22 July 2005 / Published online: 8 December 2005
© Springer-Verlag 2005

Abstract We carried out a series of molecular dynamics simulations of the hydrolysis of a model trivalent metal ion in aqueous solution. We use a dissociative model for water and examine the spontaneous speciation of M^{3+} into $M(OH)_n^{(3-n)+}(n = 1, 4)$ both in neutral solution and as a function of added protons and hydroxide ions. The species distributions in neutral solution correspond reasonably well with those expected for real trivalent metal ions at neutral pH. However, the change in the species distributions as a function of either added protons or hydroxide ions is much less than expected with very large concentrations of protons or hydroxide ions required to shift the species equilibria in either direction. The influence of added protons and hydroxide ions on the species distributions appears to be proportional to the average charge of the hydrolysis couples, being highest for the 3+/2+ couple and lowest for the 1+/0 and 0/1- couples. Proton exchange rates vary with proton/hydroxide ion concentration giving a minimum at intermediate values ($[H+] \approx 0.166$) with increasing rates at both lower and higher pH.

Keywords Hydrolysis · Trivalent ion · Molecular dynamics · pH · Amphoteric · Simulation · Titration

1 Introduction

Most trivalent cations are extensively hydrolyzed in aqueous solution according to the reaction:

$$M(H_2O)_n^{3+} \leftrightarrow M(OH)_n^{(3-n)+} + nH^+ \quad (1)$$

J. R. Rustad (✉)
Department of Geology, University of California, Davis
Davis, CA 95616, USA
E-mail: jrrustad@ucdavis.edu
Tel.: +1-530-7546021
Fax: +1-530-7520951

W. H. Casey
Department of Chemistry, University of California, Davis
Davis, CA 95616, USA
E-mail: whcasey@ucdavis.edu

In dilute solutions, these reactions produce a series of $M(OH)_n$ ($n = 1$–4) hydrolysis species with populations that depend on solution pH [1]. Hydrolysis species polymerize into extended polynuclear structures at higher metal ion concentrations, further complicating observed species distributions. Hydrolysis chemistry is clearly fundamental to the behavior of trivalent metal ions in water [2].

To gain further insight into metal ion hydrolysis, we report the results of a series of molecular dynamics simulations of the titration of a model M^{3+} ion in solution. The approach is transparent: the distribution of the $M(OH)_n$ species is simply recorded as a function of the amount of protons and hydroxide ions added to the solution. The questions addressed in this paper are:

(1) What are the lifetimes of the hydrolysis species formed in the model system?
(2) How is the distribution changed by adding acid and base and how does this relate to the normal definition of pH in terms of $-\log[H^+]$?
(3) What length of a trajectory is required to obtain reproducible species distributions?
(4) Is there a systematic size dependence of the observed distributions of hydrolysis species?
(5) What is the calculated temperature and pressure dependence of the simulated hydrolysis distributions?

Most importantly, we are interested in the extent to which the various hydrolysis species manifest themselves in the model system, and whether, in an overall sense, the behavior of the model is reasonable in terms of what is currently known about metal ion hydrolysis.

Previous attempts to model metal ion hydrolysis have proceded indirectly, usually through calculation of gas-phase or continuum-solvent proton affinities [3]. In [4], a free-energy perturbation approach was attempted within the context of the same model used here. With the increase in computer power over the past decade, it is now reasonable to attempt to calculate the hydrolysis species distributions directly.

2 Methods

2.1 General approach

In this study, populations of the hydrolysis species $M(OH)_n$ ($n = 1, 4$) are computed in aqueous solution as a function of added protons or added hydroxide ions. We begin with the general expression for the equilibrium constant:

$$K_{1n} = \frac{\gamma_{M(OH)_n^{(3-n)+}}[M(OH)_n^{(3-n)+}]\gamma_{H^+}[H^+]}{\gamma_{M(OH)_{(n-1)}^{\{3-(n-1)\}+}}[M(OH)_{(n-1)}^{\{3-(n-1)\}+}]} \quad (2)$$

which can be rearranged to give:

$$pH* = pK_{1n} + \log\frac{[M(OH)_n^{(3-n)+}]}{[M(OH)_{n-1}^{\{3-(n-1)\}+}]} + \log\frac{\gamma_{M(OH)_n^{(3-n)+}}}{\gamma_{M(OH)_{(n-1)}^{\{3-(n-1)\}+}}} \quad (3)$$

where pH* is the apparent pH of the solution. Equation (3) shows that pH* can be estimated from the hydrolytic speciation of the metal ion and the known pK_{1n} of the metal ion (the 1 preceding the n means that the species involved are monomeric, which is always the case in this study). For example, the first hydrolysis constant for Fe(III), pK_{11}, is $\approx$ 2.2. If, in simulation with n added protons, we should find that the concentration ratio of $[M(OH)(H_2O)_5^{2+}]/\ [M(H_2O)_6^{3+}]$ is nearly unity, then (ignoring activity corrections) the apparent pH (pH*) would be close to 2.2. The last term in Eq. (3) depends, in general, on the concentration of all the ions in solution.

2.2 Molecular dynamics protocol

The calculations were carried out using Nose–Hoover molecular dynamics methods [5]. The code is the same as that used in previous publications [6,7]. This code uses the Ewald summation method [7,8] to calculate energies and forces for a system of charges and inducible point dipoles. Standard units for classical molecular dynamics simulations of charged systems were employed: Length (Å); Mass (a.m.u.); Energy (e^2/Å, 332.06386 kcal/mol). In these units, the time unit is 2.6828×10^{-15} s. Henceforth, such units will be referred to as MDU. Also as in previous publications, the polarization degrees of freedom are treated using an extended Lagrangian method derived from [9]. The fictitious dipole mass is 0.1 MDU.

The ions are maintained at an average temperature of 400 K and the dipolar degrees of freedom are thermostatted at 5 K. The simulations were run at 400 K to facilitate equilibration on available time scales, which was questionable in previous studies at 300 K [10]. The problems associated with momentum conservation in two-thermostat systems [11] are treated by setting the total ion momentum to zero every 500 steps. Henceforth, let us refer to the resulting ensemble as NVT*. The ensemble is somewhat unphysical in that coupling between OH vibrations and dipole oscillations continually leak spectral power from the OH vibrations. This power is reintroduced into the low-frequency region of the spectrum through the ion thermostat. The structure of the system, as indicated by the pair correlation functions, remains stable and time-independent for trajectories in excess of 10 ns (longer trajectories were not tested here). Simulation parameters are given in Table 1.

2.3 Potential model

The potential functions are taken from [4] with minor modifications. The potentials were developed for Fe^{3+}, however, subsequent research has shown that simple models such as the one used here are probably not capable of distinguishing trivalent metals with M–O bond lengths of 1.9–2.1 Å. It is well known, for example, that hydrolysis constants for trivalent ions do not correlate with bond length [12]. Anything more subtle than a size/charge reactivity trend is probably beyond the capabilities of the type of model used here. In subsequent discussion we refer to M, the model ion, without assigning it to a particular element. The examples we discuss refer to ferric iron hydrolysis.

The O–O, O–H, and H–H interactions are taken from [6]. The functional form of this potential is basically that of [13, 14]. The model consists of +1 and −2 charges on the proton and the oxide ion, and an inducible point dipole centered on the oxygen ion. The potential differs from other water potentials in that the point dipole feels the electric field of the bound protons. As described in more detail in [6], short ranged O–H interactions are applied to recover the known structure, heterolytic dissociation energy, dipole moment, and vibrational frequencies of the isolated water molecule. O–O interactions were chosen to reproduce as closely as possible the O–O radial distribution function as measured in [15]. For this model, the ambient pressure at room temperature is about 0.7 GPa. The dielectric constant has not been calculated, but the average water dipole moment at 300 K in pure water is close to three Debye, in good agreement with estimates from density functional methods [16]. The proton in water yields

Table 1 Run-time parameters for the simulations

Mass of M^{3+}	27
Mass of O^{2-}	16
Mass of H^+	2
Fictitious dipole mass	0.1
Mass of ion thermostat	50
Mass of dipole thermostat	10
Dipole Temperature	5 K
Time step	0.1 (0.268 fs)
αL_{box}	6
L_{box} (small system)	24.8304 Å
L_{box} (large system)	29.8500 Å

Units are in MDU as discussed in the text

a Zundel $H_5O_2^+$ structure, while the hydroxide ion yields a subequal mixture of $OH(H_2O)_3^-$ and $OH(H_2O)_4^-$ species.

The potential expressions are given as follows:

$$\Phi_{OO}(r_{OO'}, \boldsymbol{\mu}_O, \boldsymbol{\mu}_{O'}) = \frac{1}{2}\sum_O\sum_{O'}\frac{A_{OO}}{r_{OO'}^{12}} + \frac{B_{OO}}{r_{OO'}^{6}} + \frac{4}{r_{OO'}} - \frac{2(\boldsymbol{\mu}\cdot\boldsymbol{r}_{OO'})}{r_{OO'}^3} + \frac{1}{2}\frac{\boldsymbol{\mu}_O}{r_{OO'}^3}\left(I - \frac{3\boldsymbol{r}_{OO'}\boldsymbol{r}_{OO'}}{r_{OO'}^2}\right)\boldsymbol{\mu}_{O'}, \quad (4)$$

$$\Phi_{OH}(r_{OH}, \boldsymbol{\mu}_O) = \sum_O\sum_H a_{OH}\frac{e^{-b_{OH}r}}{r_{OH}} + \left\{c_{OH}\left(r_{OH} - r_{0_{OH}}\right)^2 - d_{OH}\left(r_{OH} - r_{0_{OH}}\right)\right\}e^{-e_{OH}\left(r_{OH}-r_{0_{OH}}\right)^2} - \frac{2}{r_{OH}} - \frac{\boldsymbol{\mu}_O\cdot\boldsymbol{r}_{OH}}{r_{OH}^3}S_{OH}(r_{OH}), \quad (5)$$

where

$$S_{OH}(r) = \frac{r^3}{r^3 + f(r)}, \quad (6)$$

and

$$f(r) = \frac{f_{OH}\left(r - r_{0_{OH}}\right)e^{-g_{OH}\left(r-r_{0_{OH}}\right)} + h_{OH}e^{-p_{OH}r}}{1 + e^{s_{OH}(r-t_{OH})}}, \quad (7)$$

$$\Phi_{HH} = \frac{1}{2}\sum_H\sum_{H'}\frac{1}{r_{HH'}}, \quad (8)$$

$$\Phi_{HOH} = \sum_O\sum_H\sum_{H'}\left\{\begin{array}{l} a_{HOH}(r_{OH} - r_{0_{OH}})(r_{OH'} - r_{0_{OH}}) \\ +\frac{1}{2}b_{HOH}(\theta - \theta_0)^2 + c_{HOH} \\ \left(r_{OH} + r_{OH'} - 2r_{0_{OH}}\right) \\ \times(\theta - \theta_0) + d_{HOH}(\theta - \theta_0)\end{array}\right\} \times e^{-e_{HOH}\left\{(r_{OH}-r_{0_{OH}})^2 + (r_{OH'}-r_{0_{OH}})^2\right\}}. \quad (9)$$

As described in more detail in [4], the M–O potential function was fitted to quantum mechanical calculations on the Fe^{3+}–H_2O potential surface [17]. The functional form allows for polarization of bound water molecules by the M^{3+} ion. This polarization opposes the contribution of the protons to the induced dipole moment of bound water molecules. As mentioned previously, a consequence of Eq. (5) is that protons induce a dipole moment in the oxide ion to which they are bound; this is an essential feature of the dissociating water model, but this interaction is normally not explicitly considered in other non-dissociating polarizable water models. The *total* dipole moments of the bound water molecules (induced moment plus moment due to O^{2-} and $2H^+$) are thus *larger* than that of unbound water molecules. In [4] it was shown that the enhanced (repulsive) dipole–dipole interaction among bound water molecules is an important many-body effect in stabilizing octahedral coordination for Fe_{aq}^{3+}.

The functional form of the M–O interaction is:

$$\Phi_{MO}(r_{MO}, \boldsymbol{\mu}_O) = \sum_M\sum_O A_{MO}e^{-B_{MO}r_{MO}} + \frac{c_{MO}}{r_{MO}^{12}} - \frac{6}{r_{MO}} + \frac{3(\boldsymbol{\mu}\cdot\boldsymbol{r}_{MO})}{r_{MO}^3}S_{MO}(r_{MO}), \quad (10)$$

$$S_{MO}(r) = 1 - \frac{1}{e^{E_{MO}(r-F_{MO})} + 1}. \quad (11)$$

The energy required to remove a proton from the $M(H_2O)_6^{3+}$ ion is 42 kcal/mol. This is higher than calculated for $Fe(H_2O)_6^{3+}$ (19–28 kcal/mol) [3,18] but close to high-level electronic structure calculations on $Al(H_2O)_6^{3+}$ ion [19]. This is why we must be content with designating the metal ion as "M". Until the hydrolysis trends for trivalent metal are understood, there is little justification for trying to differentiate them with a parameterized model such as this one. The parameters in Eqs. (4)–(11) are given in Table 2.

2.4 Systems investigated

The majority of these calculations were carried out on the $M(OH)_3$ ion in ≈ 494 water molecules. For the alkaline titrations, n protons were removed leaving $(494 - n)$ water molecules and $n OH^-$ ions. For the acid titrations, n protons were added to the solution. To assess the system size-dependence of the population fluctuations, a series of calculations was carried out on larger systems involving an $M(OH)_3$ in 878 water molecules. In the acidic solutions, runs were carried out for $n_{H+} = 13, 11, 9, 7, 5$, and 3 for $n_{water} = 494$ and $n_{H+} = 12, 9, 6$, and 3 for $n_{water} = 878$. In basic solutions, $n_{OH-} = 7, 5, 3$, and 1 for $n_{water} \approx 494$ and $n_{OH-} = 6$ and 3 for $n_{water} \approx 878$. Note that n_{water} changes slightly with n_{OH-} because, as specified above, protons are removed from the water molecules to make OH^-; n_{water} is strictly constant for the acidic solutions.

Table 2 Potential parameters for Eqs. (4)–(11)

A_{OO}	2.02	a_{HOH}	−0.640442
B_{OO}	1.35	b_{HOH}	0.019524
		c_{HOH}	−0.347908
a_{OH}	10.173975	d_{HOH}	−0.021625
b_{OH}	3.69939	e_{HOH}	16.0
c_{OH}	−0.473492	θ_{HOH}	104.45
d_{OH}	0.088003		
e_{OH}	16.0	A_{MO}	297.44
f_{OH}	1.3856	B_{MO}	3.8455
g_{OH}	0.01	C_{MO}	1.0
h_{OH}	48.1699	E_{MO}	1.0
p_{OH}	3.79228	F_{MO}	1.8
s_{OH}	3.0		
t_{OH}	5.0		
r_{0OH}	0.9584	α	1.444 Å^3
q_H	+1		
q_O	−2		
q_M	+3		

Units are in MDU as discussed in the text

Table 3 Species distributions in acidic solution for each indicated mole fraction of protons

Soln	X_{H+}	Species $n, m (n = H_2O, m = OH)$											$pH_{0,1}$	$pH_{1,2}$	$pH_{1,3}$
		6,0	5,0	5,1	4,1	3,1	4,2	3,2	2,2	3,3	2,3	1,3			
	0.022	4503	11	20599	153		4557	123		48	6		2.85	2.83	4.39
	0.022	4761	7	22150	124		2900	54		4			2.86	2.6	3.46
	0.018	4144	3	20073	119		5457	125		78	1		2.88	2.92	4.48
	0.018	3243	3	20209	117		6112	148		139	29		2.99	2.97	4.76
	0.018	1356	3	23185	165		5140	107		41	2		3.43	2.83	4.24
	0.015	1134	3	20060	119		8409	161		108	6		3.44	3.11	4.45
	0.015	1308		21918	125		6463	90		94	2		3.42	2.95	4.5
	0.015	1257	2	21070	140	1	7215	186	2	122	5		3.42	3.02	4.56
HT	0.015	1244	4	19744	236	2	7552	314	10	155	14		3.39	3.08	4.66
LG	0.012	169		15848	119		13039	375	3	425	20		4.17	3.4	4.85
	0.011	805		18953	99		9689	246	2	194	10		3.56	3.2	4.64
HT	0.011	466	3	16679	155	1	11822	572	18	224	56	4	3.75	3.35	4.69
LG	0.009	275		13807	80		15146	324	2	342	22		3.89	3.53	4.7
	0.007	234		18915	108	3	10375	228	3	129	5		4.1	3.23	4.43
	0.007	808	4	14192	65	3	14443	295	3	180	10		3.43	3.49	4.44
HT	0.007	813	2	17484	202		10867	442	9	168	13		3.53	3.29	4.53
LG	0.005	145		14684	93		13150	304	2	1519	101	2	4.2	3.44	5.41
HD	0.003	24	1	9009	43		19974	519	3	377	44	4	4.75	3.83	4.65
	0.003	117		16088	93		13034	353	4	297	13	1	4.33	3.4	4.7
	0.003	32		9751	64		19347	446	2	341	17		4.68	3.78	4.59
HT	0.003	43		12343	129		16410	745	22	261	44	3	4.65	3.62	4.58
LG	0.002	14		9114	42		18031	397	3	384	15		5.01	3.78	4.67

Configurations were collected every 100 time steps. *LG* indicates *n* water=878; *HT* indicates a run at 450 K, *HD* indicates a run at high density, as discussed in text

Table 4 Species distributions for neutral solutions

Soln	Species $n, m (n = H_2O, m = OH)$											$pH^*_{1,2}$	$pH^*_{2,3}$	$pH^*_{3,4}$
	5,1	4,1	4,2	3,2	2,2	3,3	2,3	1,3	2,4	1,4	0,4			
LG	243	6	16585	413	6	9315	1311	97	18	6		5.31	6.13	6.95
LG	225		13372	297	3	12275	1746	51	26	1		5.26	6.34	6.88
	85		8944	57		19202	1554	15	130	8		5.5	6.69	7.42
	14		8946	10		19682	1177	11	155	5		6.29	6.7	7.48
LD	77	1	6520	156	6	19887	3153	180	15	4		5.41	6.87	6.51
HD	143	1	11644	312		15777	2015	77	26	5		5.4	6.5	6.83
	78		5731	220	3	20726	2953	195	58	11		5.36	6.93	7.06
HT	79		11227	103		16229	2142	52	142	19	7	5.64	6.54	7.56

Configurations were collected every 100 time steps. *LG* indicates $n_{water} = 878$, *HT* indicates a run at 450 K, *HD* indicates a run at high density, as discussed in the text

For most runs, the volume was kept at 15309.15 $Å^3$, corresponding to a number density, for water, of 31.24 $Å^3$ (0.9568 g/cm^3) in the $n = 0$ system. Each run was repeated 2–3 times, including a 500 K re-equilibration run to mix the system more thoroughly. The effect of small changes in density were assessed for the neutral system for volumes of 14976.47 $Å^3$(0.9781 g/cm^3) and 15773.04 $Å^3$(0.9286 g/cm^3). Several calculations at 450 K were carried out on the 494-water system to investigate the effect of temperature on the hydrolysis populations.

Because the Ewald summation was employed, these simulations have an implicit uniform background charge balancing any uncompensated hydroxide ions and protons in the simulation cell (i.e. those protons and hydroxide ions added to the neutral solution). While it would be interesting to examine the effect of adding explicit counterions, our preliminary work suggested that explicit counterion effects are small [10]. The implied background charge is a useful model for a noninterfering background electrolyte in small systems such as these [20].

The species distributions were determined through cutoff radius criteria based on calculated radial distribution functions. O^{2-} were considered bonded to the M^{3+} ion if r_{MO} was less than 2.5 Å. Protons were considered bonded to O^{2-} if r_{OH} was less than 1.2 Å.

3 Results

3.1 Simulated population distributions

The main results of the calculations are summarized in Tables 3, 4, and 5. These tables give the populations of hydrolysis species as recorded over the last 750 picoseconds of each nanosecond (ns) run. The tables therefore represent over 40 ns of total simulation time. The species are identified by n, m

Table 5 Species distributions for basic solutions

Soln	X_{OH-}	Species $n, m (n = H_2O, m = OH)$												$pH_{2,3}$	$pH_{3,4}$
		5,1	4,1	3,1	4,2	3,2	2,2	3,3	2,3	1,3	2,4	1,4	0,4		
	0.003	64			7924	12		20630	569	8	768	25		6.76	8.17
	0.002	81	1		6777	200		14307	2141	134	782	485	592	6.71	8.65
LG	0.004	95			6626	179		19169	2335	150	978	292	149	6.83	8.42
LG	0.004	112			6157	126	3	19214	2499	124	1037	495	232	6.87	8.51
	0.006	64	4	1	6102	161	2	19804	3052	169	756	299	305	6.9	8.37
	0.006	38			2748	104		19200	2717	113	1025	52	3	7.22	8.29
HT	0.006	77			5051	302	7	18665	3607	414	1268	382	326	6.96	8.54
LG	0.007	89	1		5677	186	2	19564	2616	161	1245	330	129	6.91	8.48
	0.01	86			4600	113		20058	2367	118	1944	549	165	7.01	8.67
	0.01	27	2		2671	104		21165	3208	185	1888	406	343	7.28	8.63
	0.011	67			5643	254	5	17288	3729	422	1962	409	220	6.89	8.68
	0.014	38	1		2902	84	2	19647	2550	118	3792	570	285	7.2	8.92

Configurations were collected every 100 time steps. *LG* indicates $n_{water} \approx 878$, *HT* indicates a run at 450 K, *HD* indicates a run at high density, as discussed in the text

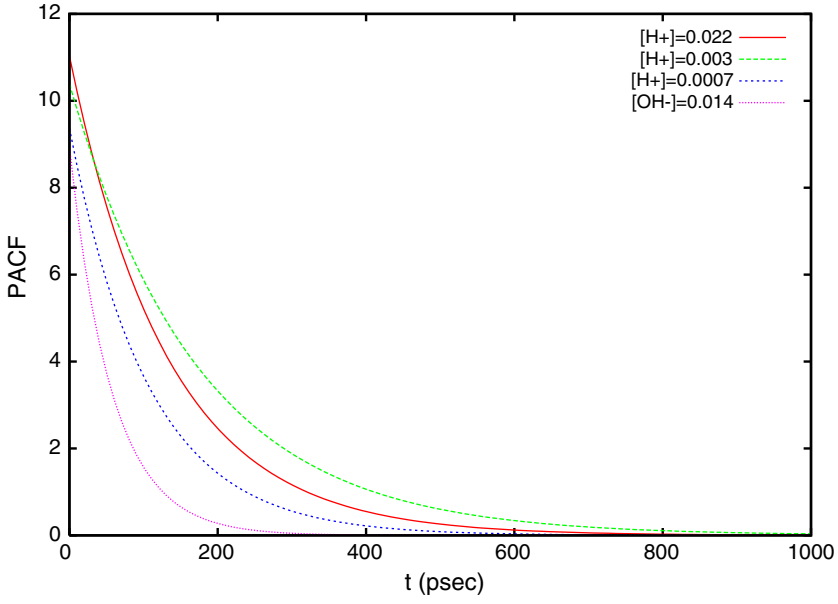

Fig. 1 Proton association correlation function as a function of $[H^+]/[OH^-]$

where n is the number of water molecules attached to the complex and m is the number of hydroxide ions attached to the complex. Unless otherwise indicated in the first column, calculations were carried out on the 494 water systems at 400 K and a water number density of 31.24 $Å^3$/water molecule(0.9568 g/cm^3). An entry of HT in column 1 indicates a run carried out at 450 K, and entry of HD indicates a run carried out at a number density of 30.56 $Å^3$/water molecule(0.9781 g/cm^3), LD indicates a number density of 32.19 $Å^3$/water molecule(0.9286 g/cm^3), LG indicates a large system ($\approx$ 878 water molecules).

3.2 Rates of proton exchange

A key factor in this simple approach is whether there is a sufficient number of proton exchanges for the complexes to provide meaningful averages on available time scales. Tables 3, 4, and 5 show the populations, but not the characteristic time scales for exchange. To convey this information we define the "proton association correlation function" (PACF): given a list of protons associated with the complex at time t_0, $H_n^+(t_0)$, the PACF, $P(t)$, gives the number of protons remaining on the list at time t. After the PACF has decayed to zero, all the protons have been exchanged from the complex. Figure 1 shows the variation of the PACF with pH*. This figure was produced by fitting $P(t)$ to an exponential function $A_n e^{-\lambda t}$ where A_n is the average number of protons associated with the complex at t_0. The characteristic exchange times ($1/\lambda$) are given in Table 6. As expected, there is a strong dependence of λ on the apparent pH. Generally, one expects $1/\lambda$ to decrease with increasing pH*, as exchange from a hydrolyzed species would be expected to be more rapid than from the fully protonated ion. Our results show a slight minimum between $X_{H+} = 0.022$ and $X_{H+} = 0.0007$, that is, the rate of proton exchange actually increases with decreasing pH* at some

Table 6 Characteristic timescales for proton exchange determined by fitting the proton association correlation function to $A_n e^{-\lambda t}$ where A_n is the averate protonation state at the indicated proton/hydroxide ion concentration

Conc. ([H^+] or [OH^-])	$1/\lambda$(ps)	λ(1/ps)
0.022[H^+]	133	0.0075 ± 0.0001
0.003[H+]	175	0.0057 ± 0.00007
0.0007[H+]	106	0.0094 ± 0.0003
0.014[OH−]	57	0.0174 ± 0.0003

point below pH* ≈ 4–5 (see below). A similar minimum in proton exchange rate as a function of pH has been observed in ^{1}H NMR spectroscopy on rhodium(III) in aqueous solutions [21].

A couple of caveats must be discussed in the context of proton exchange rates. We remind the reader that these simulations employ purely classical dynamics and purely classical distinguishable protons. Thus, the results cannot be quantitative. Moreover, our NVT* two-thermostat system is by no means dynamically consistent. Because of the continual removal of energy in the high frequency spectrum and its reintroduction into the low frequency spectrum, the "time" is not really meaningful. One could in fact view this ensemble as preferentially exciting low-frequency degrees of freedom and thus preferentially following low energy vibrational modes that might be more likely to yield transition paths than in a Boltzmann-sampled ensemble. This may be part of the reason why our simulated exchange times, if taken at face value, are so fast relative to experiment (picoseconds in the simulation versus milliseconds from experiments on several trivalent ions [21–23]. Nevertheless, the PACF serves as an important qualitative benchmark of ergodicity in our simulations.

3.3 Hydrolysis with no added protons or hydroxide ions

We discuss our results using the hydrolysis constants of ferric iron to estimate pH*: $pK_{11} = 2.19$, $pK_{12} = 3.48$, $pK_{13} = 6.33$, and $pK_{14} = 9.6$ [1]. In the case where no protons or hydroxide ions are added, the pH* values estimated from Eq. (3) (with $\gamma_i = 1$) and Table 4 are within 1.5 pH units of one another. For example, the pH* estimated from pK_{12} and the $\log(M(OH)^{2+})/(M(OH)_2^+)$ varies from 5.26 to 6.29 (average value ≈ 5.5); pH* estimated from pK_{13} and $\log(M(OH)_2^+)/(M(OH)_3)$ ranges from 6.13 to 6.93 (average value ≈ 6.6); and the pH* estimated from pK_{14} and $\log(M(OH)_3)/(M(OH)_4^-)$ ranges from 6.5 to 7.6 (average value ≈ 7.1). The ratios yield consistent values of pH* and these ratios should ideally equal neutral pH = 7. The system size dependence appears to be quite small, although there might be a tendency for the large systems to be slightly acidic. There is no discernable temperature or density dependence.

3.4 Titration with protons and hydroxide ions

When excess protons or excess hydroxide ions are added to the solution, we expect the ratios of the hydrolysis species to shift to more acidic or basic values. It would be reasonable to expect that pH* have a rough correspondence with $-\log[H^+]$. In Fig. 2, we compare pH* (taken from Table 3) and $-\log[H^+]$ for simulations with added protons. We compute $\log[H^+]$ by taking the added protons minus the protons consumed by the complex. The number of protons consumed by the complex is computed according to:

$$H^+_{\text{cons}} = \sum_{n=0}^{n=4} (3-n) X_{M(OH)_n}. \tag{12}$$

Certainly there is little quantitative similarity between pH* and $-\log[H^+]$. Forcing $(M(OH)^{2+})/(M^{3+}) \approx 1$, which should occur at $pH = pK_{11}$ (pH ≈ 2.2) requires proton concentrations in excess of three molal, which is clearly unreasonable.

In addition, the slopes of concentrations of the hydrolyzed species ratios with pH* deviate from unity. If activity coefficients are ignored:

$$\frac{\partial \log \frac{[M(OH)_n^{(3-n)+}]}{[M(OH)_{(n-1)}^{\{3-(n-1)\}+}]}}{\partial \log[H^+]} = -1. \tag{13}$$

The $\delta pH^*/\delta \log[H^+](0.95)$ is consistent with unit slope for the $M(OH)^{2+}/M(OH)_2^+$ couple, but is clearly higher than unity for the $M^{3+}/M(OH)^{2+}$ couple (1.87), and clearly lower for the $M(OH)_2^+/M(OH)_3$ couple (0.42).

Speciation under alkaline conditions was examined by adding excess hydroxide ion and checking for the variation in relative concentration of the hydrolysis species. In this case $-\log[OH^-]$ is determined by subracting the consumed hydroxide ions from the total number of hydroxide ions added:

$$OH^-_{\text{cons}} = \sum_{n=0}^{n=4} -(3-n) X_{M(OH)_n}. \tag{14}$$

In Fig. 3 pH* (taken from Table 5) is plotted against $-\log[OH^-]$. Analogous to the acidic solutions, it takes unreasonably large concentrations of hydroxide ion to achieve appreciable changes in the ratios of hydrolysis complexes. For example, to force $(M(OH)_3)/(M(OH)_4^-) \approx 1$, which should occur at $pH = pK_{14}$ (pH ≈ 9.6) requires hydroxide-ion concentrations also in excess of molal quantities, which indicates that the hydrolysis in excess base is also insensitive to the solution composition chemistry. The variation of pH* with $-\log[OH^-]$ also deviates from unity, as was observed in simulations with excess protons. However, the slopes of the $M(OH)_2^+$–$M(OH)_3$ and $M(OH)_3$–$M(OH)_4^-$ couples (0.53 and 0.49, respectively) in alkaline solutions are similar in magnitude to the slope of $M(OH)_2^+$–$M(OH)_3$ couple in acidic solutions (0.42). This suggests that the variation of slope with hydrolysis couple depends on the charge but is similar in both acidic and alkaline solutions.

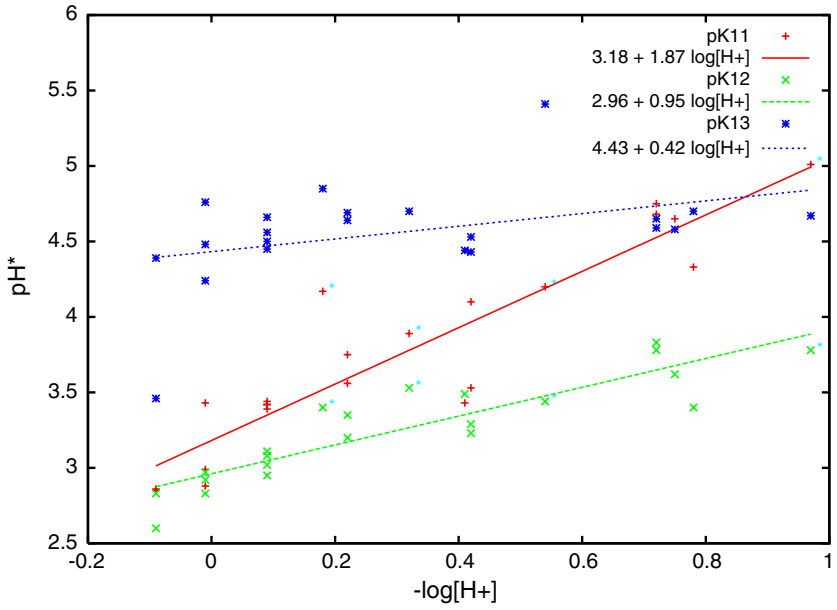

Fig. 2 Plot of pH* vs $-\log[H^+]$ for the acidic solutions. *Symbols* correspond to species distributions for $M(OH)_3/M(OH)_2^+$ (∗), $M(OH)_2^+/M(OH)^{2+}$ (×) , and $M(OH)^{2+}/M^{3+}$ (+). *Cyan asterisk* on (+) and (×) indicate that these calculations were carried out on the large system with 878 water molecules

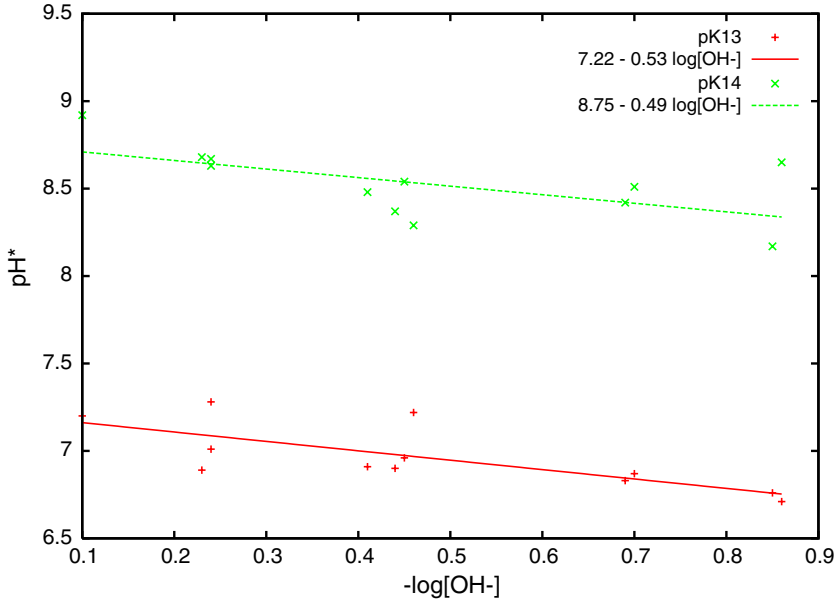

Fig. 3 Plot of pH* vs $-\log[H^+]$ for the basic solutions. *Symbols* correspond to species distributions for $M(OH)_3/M(OH)_2^+$ (+), and $M(OH)_4^-/M(OH)_3$(×)

4 Discussion

The results necessitate an explanation of both the essential correctness of the model in the neutral systems and its unresponsiveness to added protons and hydroxide ions. If the proton or hydroxide ion affinities in solution were seriously in error, then it is difficult to understand how the model system could appear reasonable in the neutral systems. This might occur if the free energies of solvation of the proton and the hydroxide ion were both large relative to the free energies of the hydrolysis reactions, but compensate one another. These affinities would have to balance closely to avoid consuming excess protons or hydroxide ions in the neutral solutions. The free energies of solution have not been calculated, however the heats of solution are approximately 240 kcal/mol for the proton and 100 kcal/mol for the hydroxide ion, which are low relative to recent estimates (262 kcal/mol for H^+ and 104.5 kcal/mol for OH^- [24]).

The slope $\frac{\partial \log \frac{[M(\mathrm{OH})_n^{(3-n)+}]}{[M(\mathrm{OH})_{(n-1)}^{\{3-(n-1)\}+}]}}{\partial \log[\mathrm{H}^+]}$ in Eq. (13) could deviate from unity because of the activity coefficient corrections representing the interaction of H^+ or OH^- with the hydrolyzed complex. The deviation will depend on the charges of the complexes as reactants and products. The ionic strength in these simulations results from the added protons and hydroxide ions, and these concentrations are high, as discussed above. The concentration of protons varies from 1.24 to 0.1 molal in the simulations. Over this range in concentrations, the ratio of the individual ion activity coefficients will differ from unity.

The slopes vary consistently as a function of the difference in charge between the two hydrolysis couples. One might expect a systematic deviation as an artefact of the electrostatic treatment, particularly involving issues associated with the uniform background charge neutralizing the H^+ or the OH^- ions. It seems that there would then be a noticeable system-size dependence. The subtrend for the large system in the acidic solution appears to be consistent with the overall slope, arguing against a systematic influence due to boundary conditions. More trajectories would certainly reduce the uncertainty, but it seems the system size effects are, if present, fairly subtle.

The common continuum models have individual-ion activity coefficients varying qualitatively as:

$$\log\left(\gamma_{\mathrm{M(OH)}_n^{(3-n)+}}\right) \propto (3-n)^2 \frac{\sqrt{I}}{1+\sqrt{I}}, \tag{15}$$

where I is the ionic strength:

$$I = \frac{1}{2}\sum m_i z_i^2, \tag{16}$$

where m_i is the molality of species i, z_i is the charge. These continuum models are inadequate at moderate to high ionic strengths (such as here), but the important point is that the activity coefficients depend on the charges for the complexes in the reaction.

The activity coefficient term, which varies with ionic strength, depends upon the absolute values of the product and reactant charges. Within the context of Eq. (15), the activity coefficient for an individual ion varies with the charge squared. For the reaction $M^{3+} + H_2O = M(OH)^{2+} + H^+$, the activity coefficient term in Eq. (2) scales like

$$\frac{\partial \log\left[\frac{\gamma_{\mathrm{M(OH)}^{2+}}}{\gamma_{M^{3+}}}\right]}{\partial \log[\mathrm{H}^+]} \propto \left(2^2 - 3^2\right), \tag{17}$$

and for: $M(OH)^{2+} + H_2O = M(OH)_2^+ + H^+$

$$\frac{\partial \log\left[\frac{\gamma_{\mathrm{M(OH)}_2^+}}{\gamma_{\mathrm{M(OH)}^{2+}}}\right]}{\partial \log[\mathrm{H}^+]} \propto \left(1^2 - 2^2\right). \tag{18}$$

Such a variation is consistent with our simulations. At a fundamental level, it appears that the effectiveness of the added protons on the hydrolysis equilibria is greater for couples of higher charge. The slopes are probably consistent with a linear variation with δz^2 of the couple, with ratios of 5, 3, 1 for couples defining pK_{11}, pK_{12}, and pK_{13}/pK_{14}, respectively.

The high density and high temperature runs exhibited no discernable variations from the baseline. The pK_{11} for Al^{3+} in aqueous solution has been measured to temperatures of 127°C [25]. The data in [25] would suggest approximately a one log unit reduction in pK_{11} for every 50° temperature increase. It seems clear from Tables 3, and 5 that we observe no temperature dependence of pK_{11} in these simulations. There might be many reasons for such behavior, however, our objective here is simply to show that our results do not appear to depend sensitively on our choice of solution conditions (errors introduced by working at 400 K are probably small, at least in terms of the internal consistency of our potential model). To our knowledge there are no experimental measurements on the pressure dependence of the pK_{11}.

5 Conclusions

Using a dissociative model for water, this paper presents an investigation of the speciation of a model trivalent metal ion in aqueous solution as a function of proton and hydroxide ion concentration. Reasonable results are obtained in neutral solutions, with hydrolysis ratios indicating an apparent pH near 7 when compared to ratios expected for Fe^{3+}. Unreasonably large concentrations of hydroxide ions or protons were required to change the distributions away from their neutral values. The variation in the ratio of hydrolysis species with proton/hydroxide addition was not uniform, being proportonal to the average charge of the hydrolysis couple. The variation was greatest for the $M(OH)^{2+}/M^{3+}$ couple and lowest for the $M(OH)_2^+/M(OH)_3$ and $M(OH)_3/M(OH)_4^-$ couples.

Our interpretation of these trends has focused on electrostatics in terms of activity coefficient corrections. However, our limited simulations on larger systems are consistent with results from those on smaller systems, although the effective ion concentrations were much lower. If the deviations that we discuss above were solely due to electrostatic contributions to free energy, we would have expected that the dilution would cause deviation from the trend established for the smaller systems as the activity coefficients relate directly to the enthalpy of dilution. Our number of large simulations is not such that we can confidently rule out electrostatic contributions, however we see no obvious system size dependence of our results. Future work will address this issue.

Characteristic hydrolysis species lifetimes show a systematic variation with the apparent pH, with a maximum at intermediate proton concentrations $pH^* \approx 4$, decreasing on either side of the maximum, in qualitative agreement with experiment [21]. Characteristic exchange times were on the order of 15 ps at the maximum and close to 5 ps at the highest hydroxide ion concentrations. These are generally much more rapid than observed in experiments on trivalent ions, but the variation with pH and the existence of a minimum in the rate of exchange with pH is encouraging within the context of the simulation.

Acknowledgements This work was supported by the Geoscience Research Program of Office of Basic Energy Sciences, US Department of Energy. We thank the Environmental Molecular Sciences Laboratory and the Molecular Sciences Computing Facility at the Pacific Northwest National Laboratory for a grant of computer time.

References

1. Baes CF, Mesmer RE (1976) Hydrolysis of cations. Wiley, New York
2. Richens DT (1997) Aquo ions. Wiley, New York
3. Rustad JR, Dixon DA, Rosso KM, Felmy AR (1999) J Am Chem Soc 121:3234
4. Rustad JR, Hay BP, Halley JW (1995) J Chem Phys 102:427
5. Allen MP, Tildesly DJ (1987) Computer simulation of liquids. Clarendon, Oxford
6. Halley JW, Rustad JR, Rahman A (1993) J Chem Phys 98:4110
7. Wasserman E, Rustad JR, Felmy AR, Hay BP, Halley JW (1997) Surf Sci 385:217
8. deLeeuw SW, Perram JW, Smith ER (1980) Proc R Soc Lond A 373:27
9. Saboungi ML, Rahman A, Halley JW, Blander M (1987) J Chem Phys 88:5818
10. Rustad JR, Rosso KM, Felmy AR (2004) J Chem Phys 120:7607
11. Morishita T, Nose S (1999) Phys Rev B 59:15126
12. Brown PL, Sylva RN, Ellis J (1985) J Chem Soc Dalton Trans 723
13. Stillinger FH, David CW (1978) J Chem Phys 69:1473
14. Stillinger FH, David CW (1980) J Chem Phys 73:3384
15. Soper AK, Phillips MG (1986) Chem Phys 107:47
16. Silvestrelli PL, Parrinello M (1999) Phys Rev Lett 82:3308
17. Curtiss LA, Halley JW, Hautman J, Rahman A (1987) 86:23219
18. Martin RL, Hay PJ, Pratt LR (1998) J Phys Chem A 102:3565
19. Wasserman E, Rustad JR, Xantheas SS (1997) J Chem Phys 106:9769
20. Blumberger J, Bernasconi L, Tavernelli I, Vuileumier R, Sprik M (2004) J Am Chem Soc 126:3928
21. Banyai I, Glaser J, Read MC, Sandstrom M (1995) Inorg Chem 34:2423
22. Fong DW, Grunwald E (1969) J Am Chem Soc 91:2413
23. Stephenson TA, Swift TJ, Spencer JB (1968) J Am Chem Soc 90:4291
24. Zhan CG, Dixon DA (2002) J Phys Chem A 106:9737
25. Palmer DA, Wesolowski DJ (1993) Geochim et Cosmochim Acta 57:2929